PERGAMON

International Journal of Heat and Mass Transfer 43 (2000) 505–520

International Journal of HEAT and MASS TRANSFER

www.elsevier.com/locate/ijhmt

An experimental study of heat transfer from a cylinder in low-amplitude zero-mean oscillatory flows

Ashok Gopinath*, Donald R. Harder [1]

Department of Mechanical Engineering, Naval Postgraduate School, Code ME/Gk, Monterey, CA 93943, USA

Received 24 August 1998; received in revised form 12 April 1999

Abstract

This is the report of an experimental study on the convective heat transfer behavior from a cylinder in an intense acoustic field which is representative of a strong zero-mean oscillatory flow. The measurements are based on a steady state technique in which, at equilibrium, a predetermined rate of heat dissipation in the cylinder is balanced by the convective cooling action of the acoustic field. Only low-amplitude cases have been treated for which the particle displacement amplitude in the oscillatory flow is small on the scale of the cylinder diameter. Two distinct flow regimes have been identified. The first regime, consistent with theory, is the laminar attached flow regime which shows the expected square root dependence of the Nusselt number, Nu, on the appropriate Reynolds number, which in this case is the streaming Reynolds number, R_s. The second regime, which is less well understood, is predicted to be an unstable regime in which vortex shedding is prevalent, contributing to higher heat transfer rates. Suitable correlations have been provided for both regimes for the case of air, and suggestions have been included to extend them to other Prandtl number gases for which they are likely to be used. This work could find application in the design of heat exchangers for thermoacoustic engines. Published by Elsevier Science Ltd.

1. Background and introduction

In the past decade or so, much interest has arisen over the promise of the applicability of the field of thermoacoustics to the development of so-called thermoacoustic engines. A review of the related concepts and ideas has been provided in a tutorial article by Swift [1]. A more current report and an account of the recent successes with this technology has also been reported by Swift [2,3]. The absence of sliding seals and the limited use of moving parts, along with the ability to operate at a large fraction of Carnot efficiencies are the principal qualities that lend to the reliability and relative simplicity of thermoacoustic engines. One of the main applications being explored is the development of a thermoacoustic refrigerator that exploits the ability of the *thermoacoustic streaming* phenomenon (Merkli and Thomann [4], Rott [5], Gopinath et al. [6]) to generate an environmentally benign useful refrigerating effect as discussed by Garrett and Hofler [7] and Garrett et al. [8]. Such refrigerators have been successfully constructed with moderate cooling powers for laboratory studies, as well as with higher cooling powers for other on-site applications (see [2,3]). A similar effect has also been quite successfully exploited in pulse-tube refrigeration technology based on Stirling/Malone-type cycles to generate very low temperatures for the relatively lower heat loads required in typical cryogenic applications (Radebaugh [9]). The central idea in all these engines is the ability to convert energy from *oscillatory* fluid

* Corresponding author.
E-mail address: gopinath@nps.navy.mil (A. Gopinath)
[1] Lieutenant Commander, US Navy

0017-9310/00/$ - see front matter Published by Elsevier Science Ltd.
PII: S0017-9310(99)00138-6

Nomenclature

a	displacement amplitude of fluid oscillation [m]
A_s	surface area of test cylinder [m^2]
c	speed of sound in the fluid [m s^{-1}]
d, D	diameter of test cylinder, resonant chamber [m]
f	acoustic excitation frequency [Hz]
Gr	Grashof number
I	DC current to cartridge heater element [A]
k	thermal conductivity of fluid [W m^{-1} K^{-1}]
Nu_d	Nusselt number based on cylinder diameter
p_m	mean fluid pressure [Pa]
P_0	pressure amplitude of fluid oscillations [Pa]
Pr	Prandtl number
q	convective heat transfer rate [W]
R_h	electrical resistance of cartridge heater element [Ω]
R_s, Re_s	streaming Reynolds number, $\varepsilon^2\Lambda^2$
R_w	center-to-surface thermal resistance [°C/W]
Re	conventional Reynolds number, $U_0 d/\nu \equiv \varepsilon\Lambda^2$
T_a	ambient fluid temperature [°C]
T_c, T_s	cylinder center, surface temperatures [°C]
U_0	velocity amplitude of fluid oscillations, $a\omega$ [m s^{-1}]
V	DC voltage across cartridge heater element [V]

Greek symbols

γ	ratio of fluid specific heats
δ	Stokes layer thickness, $\sqrt{\nu/\omega}$ [m]
ε	amplitude parameter, a/d
Λ	frequency parameter, d/δ
ν	kinematic viscosity [m^2 s^{-1}]
χ	cylinder compactness parameter, $d\omega/c$
ω	angular frequency [rad s^{-1}]

motion (typically available from a high-intensity acoustic source) to useful *time-averaged* heat transport that provides the desired refrigerating effect.

The heart of a thermoacoustic engine is considered to be the 'stack'—a stack of plates on which the time-averaged heating/cooling effect is induced by the presence of a high-intensity standing wave excited across the ends of the engine. The detailed experiments of Wheatley et al. [10] and Atchley et al. [11] clearly show the fundamental nature of this phenomenon. Further experimental studies of loading on such engines have also been conducted by Swift [12] and Olson and Swift [13], and the scalability of these engines has been considered by Olson and Swift [14] using similitude arguments. An optimum choice of the system parameters can result in a large temperature gradient across the ends of the stack of the engine, with one end being hotter, and the other end being cooler, than the ambient. In simple thermodynamic terms, the acoustic power serves as a work input to provide the heat-pumping capability against the temperature gradient which is created across the ends of the stack. As in a conventional refrigerator, heat is rejected to the ambient at the hot end of the stack, while the useful refrigerating effect is tapped at the cold end of the stack.

More recently though, research attention has turned to obtaining a detailed understanding of the various 'sub-systems' in a thermoacoustic engine which have been identified as potential bottlenecks to future development. One such 'sub-system' or auxilliary component of great importance located at each end of the stack is the heat exchanger, which is designed and positioned so as to provide an efficient means of rejecting/extracting heat from these high/low temperature ends of the stack. Some ad hoc heat exchanger designs have been explored in the past (Garrett et al. [15]) although they are still of a preliminary nature and rely on conventional knowledge for mean flows (vice oscillatory flows). It has thus been recognized and acknowledged that a poor understanding of the heat transfer mechanism in such oscillatory flows has been a crucial limiting factor in the design of an efficient heat exchanger, which in turn influences the overall performance of the thermoacoustic engine.

The efficient design of a heat exchanger for thermoacoustic engines requires a fundamentally new and sound understanding of the conventional heat transport processes in the presence of an acoustic field. There had been some early interest in the general area of the interaction of acoustic and temperature/buoyancy fields, starting with the experiments of Fand, Kaye and co-workers in the late 1950s (Fand and Kaye [16], Fand et al. [17]). Richardson [18] provided an analysis of this problem which was later improved upon by Davidson [19]. A very good review of the existing state-of-the-art in this subject at that time has been provided in a review article by Richardson [20] which includes an exhaustive literature survey of the various studies on the subject. Since then however, work in this area has been relatively limited as evidenced by the few isolated studies of, and the references in, the papers by Baxi and Ramachandran [21],

Mori et al. [22], de Vahl Davis and Richardson [23], Larsen and Jensen [24] and Peterka and Richardson [25], which are however not directly relevant to the current study as discussed further below.

More recently, the papers by Ha et al. [26] and Ha and Yavuzkurt [27] indicate an interest in this field although the results from their numerical study are intended specifically for a particular problem, and cannot, it seems, be readily generalized for wider applicability to the parameter regimes of interest here. The early paper by Fand and Cheng [28], and more recently by Ha and Yavuzkurt [29], Karanth et al. [30] and Cheng et al. [31,32], and the various references to papers therein, are examples of studies on a related topic, namely the effect of oscillations on heat transfer from a cylinder *in the presence of a mean flow*, i.e. a modulated mean flow. However the very presence of a mean flow (whether it be across, or in-line with the direction of oscillations) again does not make them relevant to the current study since the fluid physics is completely different. Another related topic, dealing however with steady axial transport in a zero-mean oscillatory flow due to the Taylor–Aris mechanism has also been treated previously by various researchers. The papers by Watson [33], Kurzweg [34], Zhang and Kurzweg [35], Kaviany [36] and Kaviany and Reckker [37] are examples of studies of the enhancement in axial heat transfer due to oscillatory pipe flow using analytical, numerical and experimental techniques. More recently Liao et al. [38] and Cooper et al. [39] have extended these ideas to low frequency, large (tidal) displacement zero-mean oscillatory flows with application to cooling of electronic components. Analytical and experimental studies were conducted to obtain correlations in terms of a suitable Nusselt number.

However all of these earlier heat transfer studies can be classified into at least two broad categories which distinguish them distinctly from the thrust of the current study. One class of these early studies dealt with the interaction of acoustic and buoyancy fields to examine primarily the relative importance of natural convection and acoustically forced convection on heat transfer behavior. This is however not an issue in the current study where, owing to the intense nature of the acoustic fields being considered (as required in a thermoacoustic engine), it becomes clear that the acoustic forcing mechanism is *the only dominant convective mechanism* (as is also verified later). The other class of flows studied in the past have dealt with the effect of oscillations on heat transfer, *in the presence of a mean through-flow*, which again is not an issue in the current situation involving a closed resonator with no net through-flow, i.e. a *zero-mean* oscillatory flow. And finally, studies dealing with the Taylor–Aris mechanism are fundamentally different in that they deal with a diffusion type enhancement of axial transport in internal duct type flows, which is different from the external flow and convective transport mechanisms that are being considered in this study. Although some of the above categories of flows have been discussed in the review paper by Cooper et al. [40], one of the striking features in all these earlier studies (not covered in Ref. [40]) is the relatively unimportant role of the steady acoustic streaming motion, which, on the other hand, is found to be the primary mode of convective transport in the current study. It is expected that for the strong acoustic fields present in a thermoacoustic engine, time-averaged phenomena such as streaming, and other associated phenomena such as periodic vortex shedding play a crucial role in determining the heat transport behavior. The importance of these transport issues in thermoacoustic engines have been recently recognized and studied by Wetzel and Herman [41] and Worlikar and Knio [42], although more from the standpoint of understanding the details of the fluid mechanics in the immediate vicinity of the stack in a thermoacoustic engine. Mozurkewich [43] has conducted a preliminary study of heat transfer from a cylinder in an acoustic field, although it appears that since too wide a range of parameters may have been covered spanning varying mechanistic regimes of transport (*including* natural convection effects), it was unfortunately not possible to clearly distinguish between the different regimes to arrive at working correlations consistent with known theories (such as, for instance, those summarized by Richardson [20]).

In the current study, a detailed effort has been undertaken to develop correlations for heat transfer from a cylinder in a low-amplitude zero-mean oscillatory flow. The cylinder is representative of a heat exchanger tube while the oscillatory flow is typical of the acoustic field in a thermoacoustic engine. The low-amplitude feature refers to oscillatory flow displacement amplitudes being small on the scale of the characteristic body dimension, i.e. the cylinder diameter. The various dimensionless parameters of importance in this range have been identified and systematically covered.

It is well known (for instance from [19,44]) that for the relatively low-amplitude cases being treated here, attached acoustic streaming flow is the dominant heat transport mechanism, and is supplanted with (small scale) vortex shedding when this basic flow becomes hydrodynamically unstable (see [45,46]). Relatively higher amplitude cases where strong vortex shedding and separated flow behavior are essential features are also important and will be treated elsewhere. The primary motivation here is to develop correlations which could be of utility in the design of heat exchangers for thermoacoustic engines. Just as standard heat transfer handbooks abound with correlations for mean

through-flows over a plethora of geometries which are applicable to conventional heat exchanger design, a modest start has been made here to develop correlations for a zero-mean oscillatory flow over a simple but vital geometry, namely the cylinder, from the viewpoint of applicability to thermoacoustic engine heat exchanger design.

2. Some preliminaries and dimensionless parameters

As noted above, this work is the report of a detailed experimental study of heat transfer from a cylinder in a low-amplitude zero-mean oscillatory flow. Despite the zero-mean nature of the flow, the convective action of the oscillatory flow can result in significant heat transport to/from a body immersed in such a flow. One of the mechanisms for heat transport in this low-amplitude regime is the strong time-averaged fluid motion (acoustic streaming) generated by the interaction of the acoustic field with the rigid boundaries. Much work has been done in the field of acoustic streaming for over a century since the early contributions of Faraday and Rayleigh—a detailed review of the field however is beyond the scope of this report and will not be attempted here. In a series of papers Westervelt, Nyborg and co-workers (Raney et al. [47], Westervelt [48], Nyborg [49]) developed a theory for the behavior of streaming flow around isolated bodies which was later firmly established by Riley [50] and Stuart [51]. A recent article by Riley [52] provides a review of the main contributions and theories in this field. The other mechanism of equal importance in this regime is one in which at high values of the appropriate Reynolds number, the attached streaming flow gives way to a periodic vortex shedding mechanism due to inherent instabilities in the flow as studied by Honji [45], Hall [46] and Sarpkaya [53]. The associated transport rates could consequently be expected to be higher than the simpler attached flow cases. However the available theories in this unstable flow regime, in spite of the low-amplitude nature of the basic flow, are understandably far more limited due to the complicated vortex shedding behavior under these conditions.

Despite the above described studies of the fluid mechanics, a survey of the heat transfer literature shows that there is little experimental backing, by way of correlations and comparisons with the available theories, to support, and extend these ideas for the various parameter regimes of interest. In particular, for the simple case of a convex object (such as a cylinder, sphere, fin, etc.) immersed in an acoustic field, representing effectively zero-mean unconfined external oscillatory flow over a bluff body, there is little experimental data to calculate the heat transfer rates for the various flow regimes that may be encountered. Richardson [20, Figs. 2, 3] provided a useful parameter map (essentially reproduced here as Fig. 1) to understand the various possible flow regimes, and it has since become clear that there is a need to be able to determine heat transfer rates in these regimes for application to heat exchanger design in thermoacoustic

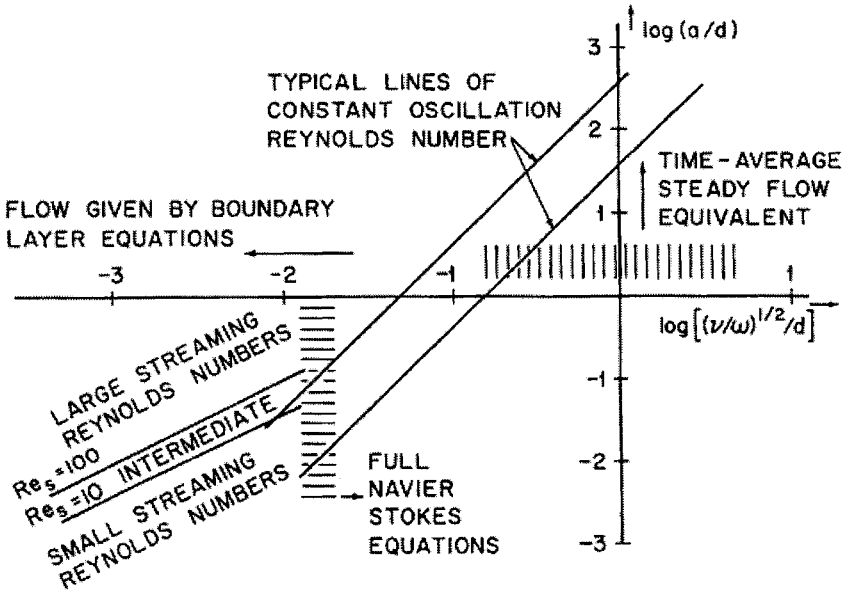

Fig. 1. Parameter map showing the different flow regimes (from [20, Fig. 2]). In the current notation the ordinate is $\log(\varepsilon)$ and the abscissa is $\log(1/\Lambda)$.

engines. A very preliminary attempt along these lines has been made in a simple experiment devised by Gopinath and Mills [44, Appendix B], although in the context of a different study. However the trends that were numerically and analytically obtained by Davidson [19] and Gopinath and Mills [44,54] in these earlier studies are expected to provide some useful insight to extend the experimental data gathered in this study.

Unlike the well known dependence on only the Reynolds number, and the Prandtl number in conventional external mean flows over isolated bluff bodies, the issue of heat transfer in an oscillatory flow is significantly more complicated due to the presence of a multitude of competing length (or time) scales. The ways in which these length scales can be ordered are many and lead to numerous distinct parameter regimes with quite drastically different flow, and hence heat transfer behavior (cf. Fig. 1). In order to perform a systematic study, it is essential to first identify the key controlling dimensionless parameters so as to be able to develop proper correlations in terms of the relevant parameters. The emphasis here is largely on parameter regimes relevant to thermoacoustic engines, with interest primarily in the net time-averaged heat transport rates induced by a zero-mean oscillatory flow.

For a cylinder of diameter d being considered, with its axis normal to the axis of oscillation of an acoustic field, the important dimensionless parameters are briefly reviewed below (see also [20]). In the compact body limit of interest, the cylinder diameter is small compared to the radian wavelength of the acoustic field and the dimensionless parameter, χ, defined as

$$\chi \equiv \frac{d\omega}{c} \tag{1}$$

is small ($\chi \ll 1$) thus making acoustic radiation effects negligible. The amplitude parameter, ε, is defined as the ratio of the displacement amplitude of fluid particle oscillation, A, to the cylinder diameter, d, and may be expressed in the following forms,

$$\varepsilon = \frac{A}{d} = \frac{U_0}{d\omega} = \frac{c}{d\omega}\left(\frac{P_0}{\gamma p_m}\right) \tag{2}$$

where the last equality is obtained from the relation that velocity amplitude, $U_0 = Mc$, where M is the Mach number and may be expressed as $(P_0/\gamma p_m)$ for a plane standing sound field. The pressure and velocity amplitudes are related by $P_0 = U_0 \varrho c$ for a standing sound field. The ratio (P_0/p_m) of the acoustic pressure amplitude to the mean fluid pressure (typically expressed as a percentage) is called the pressure ratio (or drive ratio), and is one of the primary controlling experimental variables in this study and is a measure of the strength of the acoustic field. The 'low-amplitude' feature noted in the title is precisely with reference to the above parameter, ε, and in principle refers strictly to only those cases for which $\varepsilon \ll 1$. However the basic nature of the flow field is found to be valid for values of ε up to 0.2–0.3 for which the essential nature of the low-amplitude transport features are maintained as deduced from the current experimental data. The low-amplitude data from this study will be complemented with high-amplitude data in a separate report. Also of relevance is the so-called frequency parameter, Λ^2, defined as

$$\Lambda^2 = \frac{d^2\omega}{\nu} = \left(\frac{d}{\delta}\right)^2, \quad \text{where} \quad \delta = \sqrt{\frac{\nu}{\omega}} \tag{3}$$

and is a measure of the relative sizes of the cylinder and the Stokes layer thickness. For cases of $\chi \ll 1$, $\varepsilon \ll 1$ and $\Lambda^2 \gg 1$ being considered here, it was recognized by Stuart [51] and Riley [55] that the steady (fluid and heat) transport is not governed by either of the parameters ε or Λ^2 independently, but by a suitable combination of ε and Λ^2 called the streaming Reynolds number, R_s (or Re_s), and defined as

$$R_s = \varepsilon^2 \Lambda^2 = \frac{U_0^2}{\omega\nu} = \frac{c^2}{\omega\nu}\left(\frac{P_0}{\gamma p_m}\right)^2 \tag{4}$$

where the last equality clearly shows the dependence of R_s on the experimentally measured acoustic variables, namely the frequency and the pressure amplitude (the pressure ratio), with the notable absence of the cylinder size itself. In the current study, it is this parameter R_s which is the appropriate Reynolds number which provides a measure of the forced convective effects, and not the one defined in the conventional manner as $Re = U_0 d/\nu = \varepsilon\Lambda^2$. Of interest here are cases for which $R_s \gg 1$ whereby acoustic streaming convection (vice diffusion or natural convection) is the dominant mode of steady transport. This also requires that buoyancy forces are negligible relative to forced convection effects and the appropriate criterion for this is $Gr/R_s^2 \ll 1$ (as verified later).

For the parameter regime outlined above the flow remains nominally laminar and attached only if it is hydrodynamically stable. However under certain conditions Honji [45] experimentally observed that the flow becomes centrifugally unstable resulting in separation and vortex shedding. Hall [46] has shown on the basis of a stability analysis that (to leading order) the onset of vortex shedding occurs for values of $R_s > 2.12\Lambda$ thus altering the nature of the flow. This feature has also been independently confirmed by Sarpkaya [53] on the basis of force measurements on a cylinder in oscillatory flow, by noting the distinct changes in the force coefficients associated with this flow transition. From a heat transfer viewpoint, it is

expected that such a flow transition could significantly alter (enhance) the heat transfer behavior as discussed later in this experimental study.

3. The experimental system and instrumentation

A schematic of the experimental setup is shown in Fig. 2. A heated test cylinder (representative of a heat exchanger tube) is positioned along the diameter of an enclosing cylindrical resonant chamber typical of a thermoacoustic engine configuration.

The test cylinder itself is a stainless steel cartridge resistance heater with a J-type thermocouple embedded at the midpoint along its length. In order that the surface of this test cylinder present a uniform temperature to the fluid (along its length), the cartridge heater is inserted into a very tight fitting thin walled copper sheath, which due to its high thermal conductivity serves to even the temperature along its length. A small amount of oil is introduced into the sheath (which is closed off at one end) before inserting the cartridge heater, to ensure good thermal contact in the narrow annular gap between sheath and cartridge, and thus prevent the formation of any insulatory air pockets. Although the cartridge heater has a diameter of 3.175 mm, it is of course the outer diameter of the copper sheath ($d = 5.0$ mm) which determines the effective diameter for the convection mechanism. A schematic of this cylinder-sleeve assembly is shown in Fig. 3. The cartridge heater is connected to a regulated DC power supply, while its thermocouple leads are connected to a thermocouple reader/scanner.

The outer cylindrical resonant chamber is made of a hollow plexiglass tube 2000 mm long with an inner diameter of $D = 76$ mm and a wall thickness of 6 mm. This yields a large enough aspect ratio for the test cylinder ($D/d \approx 15$), for end effects to be considered negligible. An acoustic compression driver (a loudspeaker) mounted at one end serves as the source of the acoustic excitation. The acoustic driver is connected to a waveform generator through a high-power amplifier to accurately provide the desired frequency of excitation with a variable amplitude. The other end of the resonant chamber is sealed using a piston-like end-plate which serves as a rigid end termination to provide the necessary acoustic reflection for resonance. This end plate is mounted in a piston-type arrangement (see Fig. 2) to allow its position to be adjusted so as to vary the length of the working section, and thereby allow flexibility in the choice of the resonant frequencies of operation. A washer-type seal is used to provide good acoustic confinement, and simultaneously allow easy motion of the end-plate. A through hole on this end plate is used to mount a small but sensitive pressure transducer (microphone) in such a way that its measuring face is flush with the inner face of the end plate facing the working volume of the resonant chamber. At this end-plate, the standing wave is at a velocity node, and hence a pressure antinode (peak) whose amplitude (P_0) is measured by the transducer. The transducer is connected through a preamplifier to

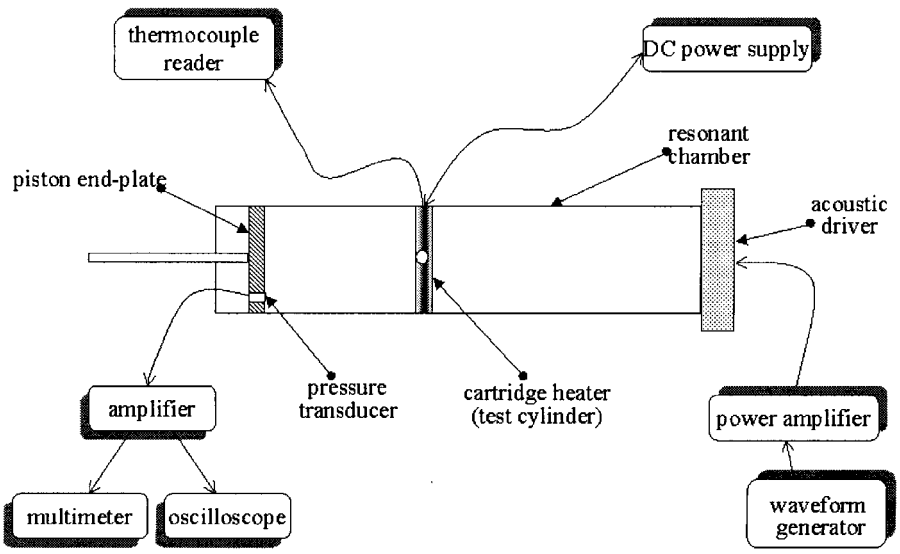

Fig. 2. A schematic of the experimental setup.

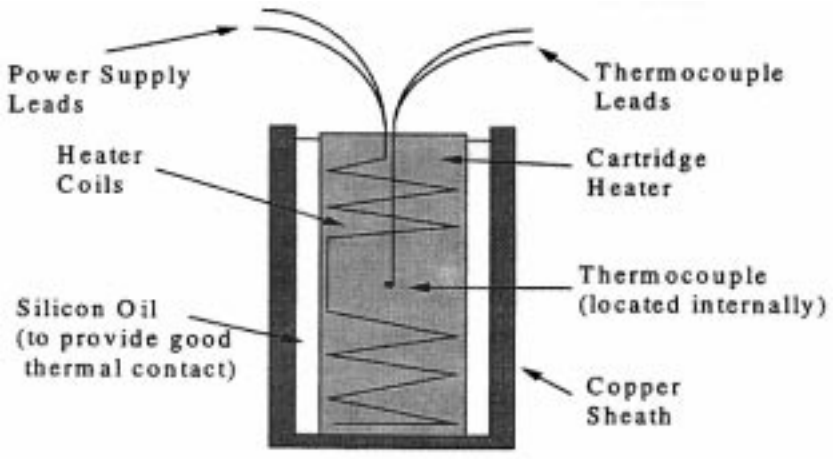

Fig. 3. A magnified schematic view of the cylinder-sleeve assembly.

a digital multimeter and an oscilloscope so as to be able to both measure the acoustic signal, and observe the acoustic waveform.

The enclosing cylindrical resonant chamber is also provided with two holes on its curved surface along its length to provide a choice of locations for inserting and positioning the test cylinder across the chamber diameter. However of course, during a given run only one of these holes is used to house the test cylinder, while the other hole is tightly plugged shut. The extra hole serves as a useful means to insert a thermocouple into the chamber to measure the air temperature soon before, and after, a run. The resonant chamber was eventually mounted with its axis horizontal, although different orientations of the test cylinder were first tried to evaluate the possible influence of natural convection (as discussed in the section below).

4. The experimental procedure

4.1. Calibration and setup evaluation

Prior to any experimentation, it was first necessary to determine the specific resonant frequencies of operation which would also ensure that the test cylinder is positioned along a velocity antinode (peak) in the standing wave. In these tests, the rigid end termination served as the obvious reference end for measuring distances since this end is a velocity node (and hence also a pressure peak) of the standing wave. It was thus necessary to determine a suitable end-plate location for which the excitation frequency would not only give rise to resonance in the acoustic chamber, but to also ensure that the position of the test cylinder would simultaneously correspond to the velocity peak at that frequency. Although this requirement was strictly not necessary for the compact body limit ($\chi \ll 1$, Eq. (1)) being considered, it was desirable to position the cylinder at such a point where the maximum 'swing' in the velocity could be achieved, and thereby also to reduce interference with the 2nd harmonic for reasons noted below. Furthermore, such a pressure node location also corresponds to the location of no Rayleigh streaming (on the chamber walls), and is hence desirable, to keep the interference between cartridge cylinder streaming and chamber wall streaming down to a minimum. At each suitable resonant excitation frequency that was identified, the maximum achievable signal amplitude (acoustic signal strength or pressure ratio) was determined. The goal was to achieve as high a pressure ratio as possible without distorting the acoustic waveform significantly from its sinusoidal nature. It is well known that such a distortion occurs with increasing signal amplification, as manifested by a steepening of the wavefront resulting in the formation of shocks caused by rapid strengthening of the harmonics. The waveform behavior was observed on an oscilloscope and also monitored by noting the strength of the harmonics with the help of a digital signal analyzer. Since the second harmonic is completely out of phase with the first (the driving frequency), and $\chi \ll 1$, the interference between these harmonics would be minimal at the location of the test cylinder *if it were positioned at the velocity peak of the first harmonic*. So the sinusoidal nature of the waveform was considered acceptable so long as the *third harmonic* (whose alternate nodes overlap with the first) had an amplitude less than 5% of the first harmonic (the driving frequency). In this manner five suitable resonant frequencies were identified for various values of the working

length, L, with the maximum achievable pressure ratio for each frequency showing a decreasing trend with increasing frequency.

In addition to satisfying the requirements for resonance as noted above, the chosen frequencies have to be below the so-called 'cut-off' frequency for this particular chamber geometry. This means that the frequencies would have to be in a range which would excite only the axial mode of the plane standing wave in the chamber, and not the higher order radial/transverse modes which are currently not of interest. This criterion indirectly dictates the choice of the chamber dimensions, since the cut-off frequency depends on the chamber length and diameter. For the current choice of chamber size, the cut-off frequency was found to be about 2.6 kHz and all the working frequencies were maintained well below this value.

The resistance of the heating element of the cartridge heater was measured using a 4-wire measurement technique. This resistance value was also confirmed by comparison with simple voltage and current readings from a DC-power supply. This resistance was found to be $R_h = (123.2 \pm 0.2)\ \Omega$ and quite invariant with temperature. For data reduction calculations, it is this resistance, along with the power supply voltage, that was used to determine the power dissipated by the resistance heater.

In the interests of maintaining a closer tolerance in the temperature uncertainties (due to the small driving temperature differences expected in the experiment), all the thermocouples that were used, including the manufacturer provided thermocouple embedded in the cartridge heater, were calibrated prior to use. The thermocouples were calibrated to measure temperature with an error of no more than 0.1°C (the least count of the thermocouple reader), which is much smaller than the usually assumed uncertainty of 0.5–1.0°C and is hence a smaller source of error in the measurements. Once calibrated, these thermocouples were also used to determine the difference in the temperature measured by the thermocouple embedded inside the cartridge heater, and the outer temperature on the surface of the copper sheath which would be the true driving surface temperature responsible for convection. This was achieved by firmly affixing three thermocouples on the outer surface along the length of the heater-sheath unit and measuring the temperature difference between the internal embedded value and the (average) surface value for a precisely known amount of power being dissipated. The heater-sheath–thermocouple assembly was suspended outside of the resonant chamber, and various temperatures and natural convection heat transfer rates in still air, comparable to those expected in the actual experiment were used to simulate true conditions as closely as possible. Additional tests were also performed using a fan to blow air across the test cylinder to simulate larger heat transfer rates while staying within the expected temperature range. In this process it was first verified that the three sheath surface temperature measurements were different from each other by no more than 0.3°C thereby justifying the role of the copper sheath in evening the surface temperature. Subsequently, the internal-to-surface temperature drop was measured and conveniently expressed in the form of an appropriate thermal resistance, R_w, which was calculated to be about 1.02°C/W. In the actual experimental runs with the acoustic field, these three outer thermocouples were of course removed from the sheath to present a smooth cylindrical surface to the flow, and it was the above resistance value, R_w, which was then used to deduce sheath outer surface temperature from measurements of the internal cartridge temperature.

Finally as noted earlier, with the test cylinder inside the resonant chamber immersed in the sound field, the influence of natural convection on the heat transfer rate was studied by examining different orientations of the chamber rotated about its axis. In this manner, with all other things being the same, the orientation of the test cylinder with respect to the gravity vector was varied and changes in heat transfer rates (if any) were studied. It was found that even for the weakest acoustic signal strength of interest used in this entire experimental study, the orientation of the test cylinder caused no significant change in the heat transfer rate thus confirming the dominance of the acoustically forced convection mechanism relative to the buoyancy mechanism. This feature was also independently confirmed by verifying that the ratio Gr/R_s^2 is indeed small and found to be no more than 2% throughout this study for the R_s values of interest (upwards of ~100).

4.2. Data collection

One of the main objectives in this experiment was to gather a broad base of reliable data to ultimately arrive at useful correlations for the Nusselt number. To this end, the measurements were conducted for five suitable resonant frequency settings, and at each such setting the pressure ratio (P_0/p_m) was varied from about 0.8% up to its maximum possible value without significantly distorting the sinusoidal waveform as per the criteria noted earlier in section 4.1. The maximum value of pressure ratio achieved in this study was about 3.2% for the 585 Hz setting.

At each frequency-pressure ratio combination, data was recorded for the test cylinder surface heated to about 8, 12 and 16°C above the ambient temperature, under steady state conditions. The associated power dissipation rates itself were found to be small, and thus would not be expected to cause any significant temperature rise of the air inside the chamber during

the course of an experimental run. In order to ensure reproducibility and eliminate any anomalistic behavior, three runs were conducted at each of the temperature points noted above to ensure consistency in the data.

A typical experimental run entailed the following. The test cylinder consisting of the heater-sheath assembly was inserted into one of the holes in the chamber making sure that it was securely seated in a shallow indentation on the opposite side, specifically machined for this purpose. With no power to the sheath encased cartridge heater, the instrument settings for the desired acoustic signal level (frequency and pressure ratio) were tuned in and then turned off. A thermocouple was then inserted into the chamber through the other hole (not holding the test cylinder) to measure the internal air temperature, and then removed and the hole plugged shut. In this quiescent state it was also verified that the temperature recorded by the embedded thermocouple in the heater was consistent with this measured air temperature. With the acoustic field absent, the power to the cartridge heater was now turned on (to a preset value) thus causing a fairly rapid rise in its temperature as indicated by the embedded thermocouple. Once the cylinder temperature had risen past its projected steady state value (estimated from experience), the acoustic field was then turned on to its previously preset value thus instantly providing the acoustically forced convective cooling action. As a result, the cylinder temperature would immediately start to drop, and quickly reach a minimum where it would stay for sometime before starting to *very slowly* climb again. The occurrence of the temperature minimum was recognized to be the desired steady state equilibrium heat balance condition, with the subsequent gradual temperature rise of the cylinder attributable to the concomitant slow temperature rise of the ambient air sink temperature in the immediate vicinity of the cylinder. Upon identification of the above desired temperature minimum signaling equilibrium, the corresponding steady state temperature values were recorded and the heater power and acoustic power were immediately turned off (in that order). A thermocouple was once again quickly inserted into the chamber to measure the enclosed air temperature, and to verify that the air sink temperature in the chamber (assumed to be effectively constant) had indeed not risen significantly. From all the runs in this study, it was found that even for the largest heater power settings (which was only of the order of a few Watts), the difference in chamber air temperature before and after a typical run was never more than 0.3°C. The air in the chamber was flushed between runs to ensure a uniform air temperature at the start of every run.

The strategy outlined above to achieve equilibrium conditions was considered more appropriate since it would allow steady state conditions to be rapidly achieved, *and identified*, without in the meanwhile causing a significant rise in the temperature of the ambient air in the chamber. This is especially important since it would be extremely difficult to monitor the ambient air sink temperature inside the chamber and in the vicinity of the test cylinder during the course of a run, without directly interfering with the transport behavior. It was thus deemed desirable to complete a given run as soon as possible to minimize the rise in air temperature during the run. In contrast to the above method, when the acoustic and heater powers had been simultaneously engaged at the start of each run, the presence of the convective cooling action right from the outset was found to considerably slow down the approach of the temperature to its steady state equilibrium condition, thus resulting in significant heating of the chamber air over that larger time period. As a result the steady state heat balance condition was never clearly identifiable in a consistent manner, and this technique was therefore rejected as unsuitable.

4.3. Data reduction

The acoustic signal data recorded were the input frequency f to the acoustic driver, and the corresponding pressure amplitude P_0 of the standing wave measured at the microphone. The fluid used throughout this study was air at atmospheric conditions, i.e. $p_m = 1$ atm. The thermal data recorded were the voltage V and current I from the power supply to the cartridge resistance heater, and its resulting steady state temperature, T_c. The air temperature around the cylinder was always recorded soon before, and after, each run to verify that there was no significant rise in its value during the course of a run as discussed in section 4.2. From this data, the Nusselt number based on the cylinder diameter was simply calculated from

$$Nu_d = \frac{q}{A_s(T_s - T_a)} \frac{d}{k} \tag{5}$$

where $q = V^2/R_h$ is the power dissipated by the heater. The cylinder (sheath) surface temperature T_s is related to the measured cartridge center temperature T_c recorded by the embedded thermocouple according to $T_s = T_c - qR_w$, where as noted earlier in section 4.1, R_w is the thermal resistance of the copper sleeve arrangement determined during calibration procedures. The other relevant dimensionless parameters such as Λ^2, ε, R_s, were calculated from the measured variables using the relations outlined earlier in Eqs. (1)–(4).

4.4. Error analysis

In order to obtain a measure of the reliability of the experimental data, an uncertainty analysis was performed for the principal parameters of interest, namely

the Nusselt number Nu_d, and the streaming Reynolds number, R_s. The root-mean-square random error propagation analysis was carried out in standard fashion using estimated and/or specified uncertainties of the basic independent variables being experimentally measured, namely, the heater voltage and temperatures to calculate the uncertainty in Nu_d, and the acoustic signal frequency and pressure amplitude to calculate the uncertainty in R_s. The results of this analysis were incorporated into the calculations for all the data points and have been provided in the form of error bars for Nu_d on some of the plots in the following section, and indicate uncertainties of no more than 10–15% in Nu_d. For R_s, this uncertainty is even smaller, and of the order of only 2–3%, and is hence not shown on these plots in the interests of maintaining clarity of the figures.

5. Results and discussion

Nearly 800 experimental runs were carried out in the course of this study to generate over 200 distinct data points for analysis. The data was gathered for five different acoustic frequencies (ranging from 585 to 1213 Hz) at pressure ratios, P_0/p_m, ranging from 0.8 to 3.2%. The resulting values of R_s as calculated from Eq. (4) ranged from 40 to 1070, while the corresponding values of Nu ranged from 8 to 40. The amplitude parameter (ε) varied from 0.05 to 0.45, and the frequency parameter (Λ) was in the range 76–110. These values may be compared with Fig. 1, a parameter map of the problem originally suggested by Richardson [20] that delineates the expected regimes of flow. The data obtained here cover the 'low-amplitude' range on this map as noted in the paper title (marked 'Large Streaming Reynolds Numbers' in Fig. 1), with the goal being to cover the different expected regimes within this range. One of these is the attached flow regime with a fairly well developed theory (but with little experimental verification to date) which much of the data here attempts to cover. The other is a regime, which though of low-amplitude, is characterized by a separated flow behavior due to inherent large Reynolds number instabilities and resultant vortex shedding of the Honji–Hall type. Some of the data

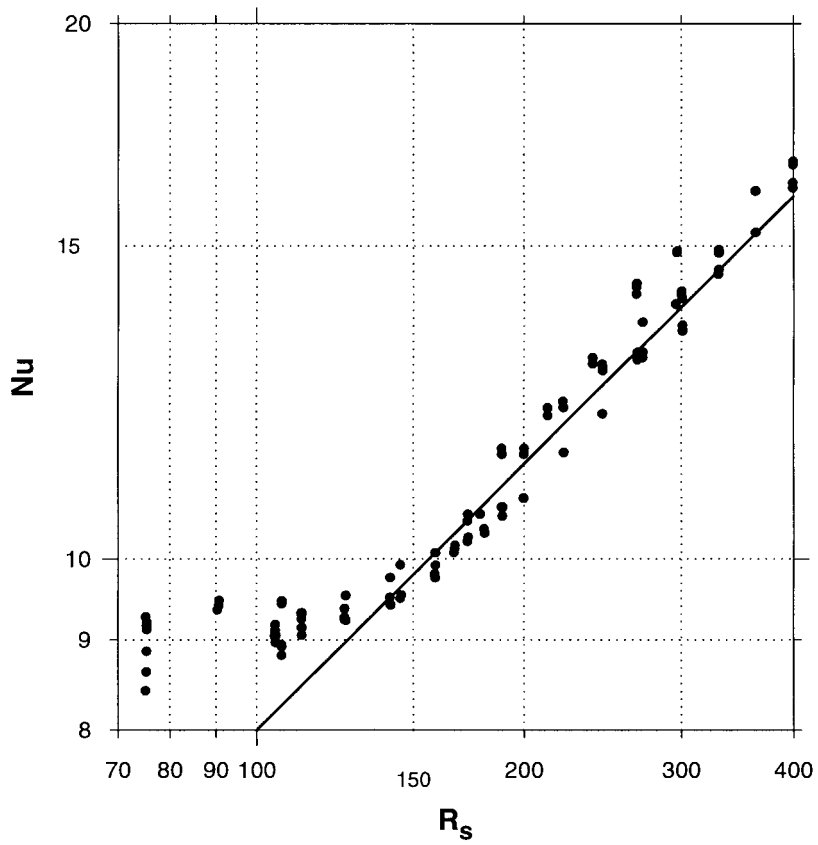

Fig. 4. Variation of Nu with R_s for $f \approx 725$ Hz ($\Lambda \approx 84.6$). The solid line is a $\sqrt{R_s}$ fit through the data.

obtained in this study also covered this regime and is discussed further below.

The results are presented in the form of plots of Nusselt number, Nu, versus the streaming Reynolds number, R_s, which from theory has been clearly identified as the appropriate Reynolds number for these low-amplitude flows. The plots are presented for each of the five resonant frequencies covered in this study, and the data accordingly correlated for each frequency. For a given frequency plot, each R_s value corresponds to a certain acoustic signal pressure amplitude as is clear from Eq. (4). And for each such R_s value the different data points come from the different ΔT settings used to determine Nu as described earlier in sections 4.2 and 4.3. The relatively small scatter in this data in the R_s range of interest attest to the accuracy of the experimental procedure.

The experimental data has been presented in Figs. 4–7 for frequencies of 725, 1055, 1213 and 585 Hz, respectively. In all of these figures the solid line represents the $\sqrt{R_s}$ curve fit expected from laminar boundary layer transport theory for 'large' values of R_s (found to be upwards of 125–150). For this R_s-range of interest, it was confirmed earlier at the end of section 4.1 that natural convection effects are indeed small compared to the forced convective effects due to the acoustic field. However, for lower values of R_s, the increased scatter in the data seems to suggest that buoyancy effects could be significant in a presumably mixed convection regime, although this behavior is not directly relevant to the goal of the current study (other than to recognize its boundary). Also, as argued earlier, the data from the different frequencies should not have to be treated independently, but should be instead all collapsible into a suitable dimensionless parameter correlation applicable to all frequencies. (For the 897 Hz frequency setting, the data obtained was far too scarce and limited to warrant an individual frequency plot, and has instead been combined with data from all the other frequencies into a final combined all-frequency data plot in Fig. 8 as discussed below.) Such a combined plot of the averaged data from all the frequencies (Fig. 8) consequently shows that the square-root dependence does indeed provide a good fit

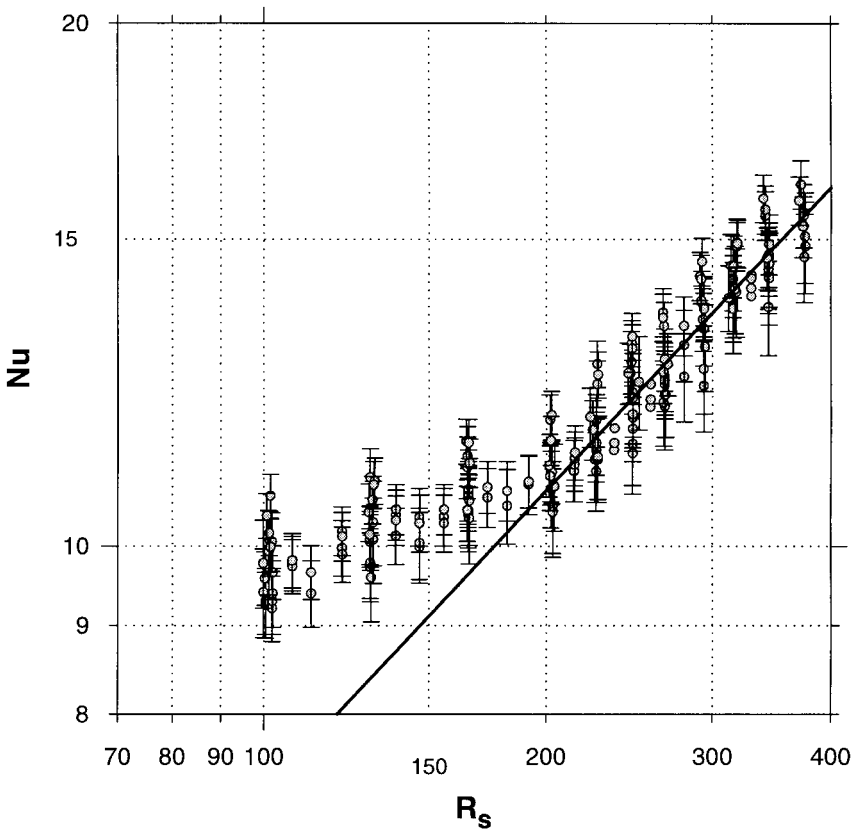

Fig. 5. Variation of Nu with R_s for $f \approx 1055$ Hz ($\Lambda \approx 102.1$). The solid line is a $\sqrt{R_s}$ fit through the data. The error bars are from a random error uncertainty analysis.

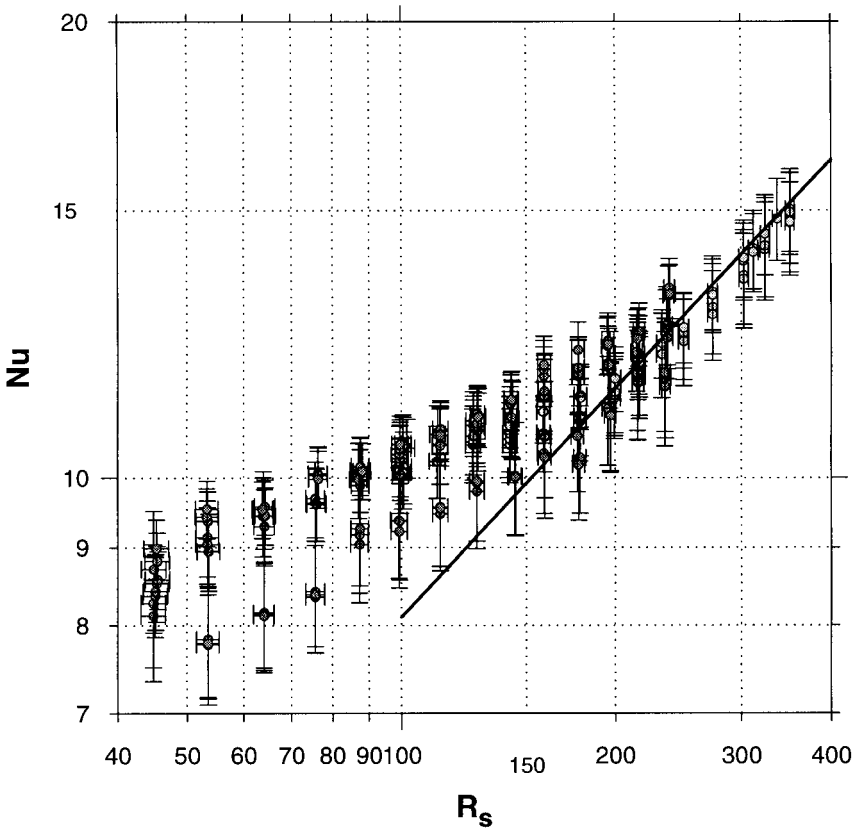

Fig. 6. Variation of Nu with R_s for $f \approx 1213$ Hz ($\Lambda \approx 109.5$). The solid line is a $\sqrt{R_s}$ fit through the data. The error bars are from a random error uncertainty analysis.

yielding a correlation with a fairly consistent leading coefficient value of about 0.90 which may be summarized as

$$\frac{Nu_d}{\sqrt{R_s}} = 0.90 \pm 10\% \quad \text{for} \quad \varepsilon \quad \text{small} \quad \text{and} \quad R_s > 125\text{–}150, \tag{6}$$

and reaffirms the choice of R_s as the appropriate parameter for the boundary layer behavior in this regime. This result may further be compared with theoretical predictions for the Nusselt number made in earlier studies for this attached streaming flow regime. The early study by Davidson [19] for a circular cylinder predicted a leading coefficient of about 1.05 for air [44, Eq. (49)], which is at the edge of the uncertainty bounds of the experimental value of 0.90 recommended from the data in this study.

The most extensive data in this study was gathered for the 585 Hz frequency value as shown in Fig. 7, which also provided the largest pressure amplitudes as indicated by the large values of R_s (up to about 1100) that were achieved. As seen from Fig. 7, the data follows two clear trends for large values of R_s—there is an initial $\sqrt{R_s}$ trend with a leading coefficient of 0.94 up to $R_s \approx 450$ which is consistent with the attached laminar flow behavior arguments made in the previous paragraph leading to Eq. (6). This $\sqrt{R_s}$ trend in the data in Fig. 7 is followed by a steeper $R_s^{3/4}$ trend for even larger values of R_s and maybe correlated as

$$Nu_d = 0.20 R_s^{0.75} \tag{7}$$

and is an unexpected trend that has not been predicted before by theory. This behavior for very large R_s values seems to suggest a more vigorous heat transport mechanism that could not be induced by laminar boundary layer convective effects alone, and may be attributable to separation in the boundary layers leading to vortex shedding and the associated increased transport rates. These experimental observations as shown in Fig. 7 are also consistent with the fluid mechanical studies of Honji [45], Hall [46] and Sarpkaya [53] in that they are clearly indicative of a change in the basic nature of the flow mechanics, possibly from an attached to a separated nature, as is evidenced here

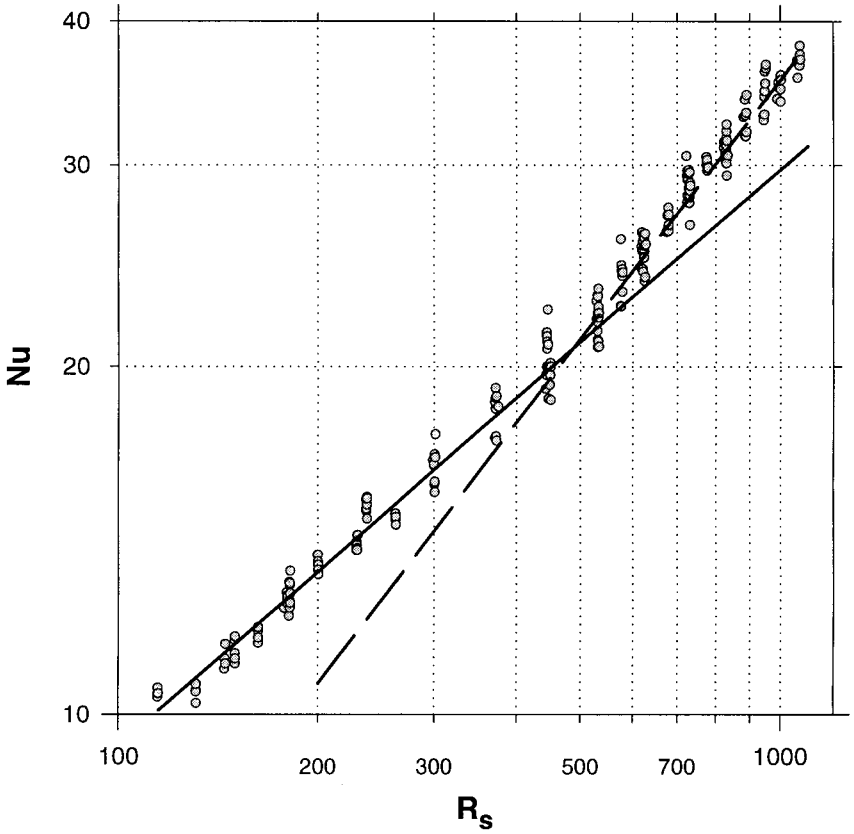

Fig. 7. Variation of Nu with R_s for $f \approx 585$ Hz ($\Lambda \approx 76.0$). The solid line is a $\sqrt{R_s}$ fit through the data. The dashed line represents the predicted $R_s^{0.75}$ behavior in the vortex shedding regime.

by the change in the power-law dependence of Nu_d on R_s. As discussed earlier, this transition is most likely attributable to instabilities in the flow which for large streaming Reynolds numbers causes the flow to become centrifugally unstable resulting in a periodic vortex shedding behavior. However the critical R_s for such a transition from attached to separated flow conditions does not seem to agree very well with the criteria laid out by Hall [46] based on his analyses. The critical R_s values predicted by Hall [46] which depend on the frequency of oscillation, vary from 150 to 250 for the choice of frequencies and other parameters in this study. However, as is clear from Figs. 4–6, there was no significant departure from the attached flow $\sqrt{R_s}$ dependence to signal such a transition, even well beyond this range of predicted critical R_s values. Only for the case of $f \approx 585$ Hz as shown in Fig. 7 was a clear change in the trend observed, and that too only at $R_s \approx 450$ which is significantly higher than the theoretical value of about 175 predicted by Hall's theory under these conditions. It may be conjectured that the reasons for this discrepancy are probably due to (a) the applicability of Hall's theory strictly to cases for which $\varepsilon \ll 1$, and/or (b) also to the confined nature of the test cylinder in the resonant chamber which therefore does not make it a truly unconfined external flow (for which again strictly the theory by Hall [46] has been developed). This latter feature could result in possible stabilizing flow mechanisms induced on the walls of the confining acoustic chamber, thus delaying the onset of criticality and transition to the vortex shedding regime of the flow on the test cylinder.

6. Conclusions

The low-amplitude nominally attached flow regime of zero-mean oscillatory flow over a cylinder has been experimentally treated to develop some useful heat transfer correlations (Eqs. (6) and (7)). The correlations developed are based on a large body of data that was gathered for the truly attached streaming flow

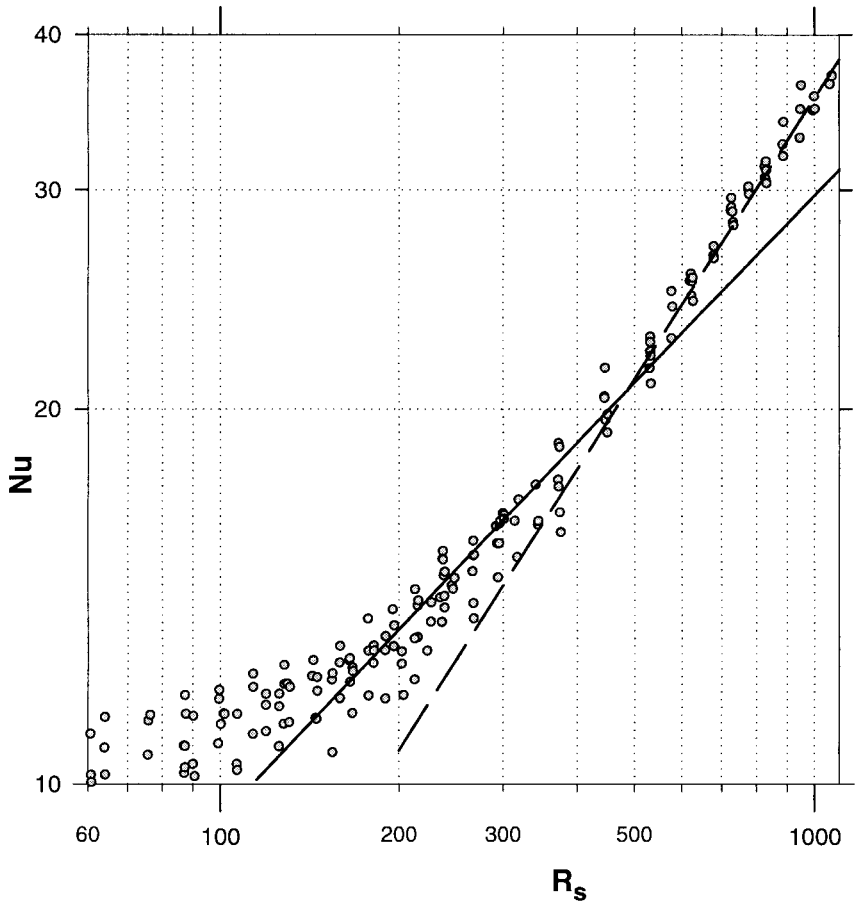

Fig. 8. A comprehensive plot of the variation of Nu with R_s for all frequencies. The solid line is a $\sqrt{R_s}$ fit through the data. The dashed line represents the predicted $R_s^{0.75}$ behavior in the vortex shedding regime.

regime, as well as for its unstable counterpart at higher R_s characterized by possible vortex-shedding behavior. It may be noted that the actual magnitude of the relevant Reynolds number, R_s, for both the attached and separated flow regimes in this study is of $O(10^2$–$10^3)$ and is considerably smaller than the values conventionally encountered in uniform mean flows which may typically range up to as high as $O(10^4$–$10^7)$. Nonetheless, as the values of the Nusselt number for these oscillatory flows indicate, the magnitudes of the heat transfer coefficients themselves (which are $O(10^2)$ W/m^2 K) are very much comparable in magnitude to those encountered in conventional mean flows, thus indicating the potential for significant convective heat transfer rates despite the zero-mean nature of the driving acoustic flow. It is suggested that when gases other than air are to be used, as is most likely the case in a thermoacoustic engine, a power-law dependence on the Prandtl number of the form $Pr^{0.7}$ established earlier by Davidson [19] and Gopinath and Mills [44,54] may be applied. This suggestion is based on the premise that such a dependence, although originally established strictly for the case of a cylinder and a sphere, should be equally suitable for other similar convex geometries which support essentially similar transport mechanisms, as is also typically assumed in conventional mean flows.

Acknowledgements

Thanks are due to Steve Garrett and Tom Hofler for their comments and suggestions on the experiment. The Reviewers' comments are much appreciated. Support from the Naval Postgraduate School and the NASA Microgravity Program is gratefully acknowl-

edged. This work is based in part on the M.S. thesis of D.R.H.

References

[1] G.W. Swift, Thermoacoustic engines, J. Acoust. Soc. Am. 84 (4) (1988) 1145–1180.

[2] G.W. Swift, Thermoacoustic engines and refrigerators, Physics Today 48 (7) (1995) 22–28.

[3] G.W. Swift, Thermoacoustic natural gas liquefier, in: Joint Meeting Acous. Soc. America, Convention of the European Acous. Assoc., German Acous. DAGA Conf., Berlin, Germany, March, 1999 (abstract in J. Acous. Soc. Am., vol. 105(2), p. 1011, February 1999).

[4] P. Merkli, H. Thomann, Thermoacoustic effects in a resonance tube, J. Fluid Mech. 70 (1975) 161–177.

[5] N. Rott, Thermoacoustics, Adv. Appl. Mech. 20 (1980) 135–175.

[6] A. Gopinath, N.L. Tait, S.L. Garrett, Thermoacoustic streaming in a resonant channel: the time-averaged temperature distribution, J. Acoust. Soc. Am. 103 (3) (1998) 1388–1405.

[7] S.L. Garrett, T.J. Hofler, Thermoacoustic refrigeration, ASHRAE Journal 34 (12) (1992) 28–36.

[8] S.L. Garrett, J.A. Adeff, T.J. Hofler, Thermoacoustic refrigerator for space applications, AIAA J. Thermophyics and Heat Transfer 7 (1993) 595–599.

[9] R. Radebaugh, Review of pulse tube refrigeration, in: Advances in Cryogenic Engineering, vol. 35, Plenum Pub Corp, New York, 1990, pp. 1191–1205.

[10] J. Wheatley, T. Hofler, G.W. Swift, A. Migliori, An intrinsically irreversible thermoacoustic heat engine, J Acoust. Soc. Am. 74 (1) (1983) 153–170.

[11] A.A. Atchley, T.J. Hofler, M.L. Muzzerall, M.D. Kite, C. Ao, Acoustically generated temperature gradients in short plates., J. Acoust. Soc. Am. 88 (1) (1990) 251–263.

[12] G.W. Swift, Analysis and performance of a large thermoacoustic engine, J. Acoust. Soc. Am. 92 (3) (1992) 1551–1563.

[13] J.R. Olson, G.W. Swift, A loaded thermoacoustic engine, J. Acoust. Soc. Am. 98 (1995) 2690–2693.

[14] J.R. Olson, G.W. Swift, Similitude in thermoacoustics, J. Acoust. Soc. Am. 95 (3) (1994) 1405–1412.

[15] S.L. Garrett, D.K. Perkins, A. Gopinath, Thermoacoustic refrigerator heat exchangers: design, analysis and fabrication, in: Tenth International Heat Transfer Conference, Brighton, UK, August, 1994, pp. 375–380.

[16] R.M. Fand, J. Kaye, The influence of sound on free convection from a horizontal cylinder, ASME J. Heat Transfer 83C (1961) 133–148.

[17] R.M. Fand, J. Roos, P. Cheng, J. Kaye, The local heat transfer coefficient around a heated horizontal circular cylinder in an intense sound field, ASME J. Heat Transfer 84C (1962) 245–250.

[18] P.D. Richardson, Heat transfer from a circular cylinder by acoustic streaming, J. Fluid Mech. 30 (1967) 337–355.

[19] B.J. Davidson, Heat transfer from a vibrating circular cylinder, Int. J. Heat Mass Transfer 16 (1973) 1703–1727.

[20] P.D. Richardson, Effects of sound and vibration on heat transfer, Appl. Mech. Reviews 20 (1967) 201–217.

[21] C.B. Baxi, A. Ramachandran, Effect of vibration on heat transfer from spheres, ASME J. Heat Transfer 91 (1969) 337–344.

[22] Y. Mori, M. Imabayashi, K. Hijikata, Y. Yoshida, Unsteady heat and mass transfer from spheres, Int. J. Heat Mass Transfer 12 (1969) 571–585.

[23] Davis G. de Vahl, P.D. Richardson, Natural convection in a sound field giving large streaming Reynolds numbers, Int. J. Heat Mass Transfer 16 (1973) 1245–1265.

[24] P.S. Larsen, J.W. Jensen, Evaporation rates of drops in forced convection with superposed transverse sound field, Int. J. Heat Mass Transfer 21 (1978) 511–517.

[25] J.A. Peterka, P.D. Richardson, Effects of sound on local transport from a heated cylinder, Int. J. Heat Mass Transfer 27 (9) (1984) 1511–1523.

[26] M.Y. Ha, S. Yavuzkurt, K.C. Kim, Heat transfer past particles entrained in an oscillating flow with and without a steady velocity, Int. J. Heat Mass Transfer 36 (4) (1993) 949–959.

[27] M.Y. Ha, S. Yavuzkurt, A theoretical investigation of acoustic enhancement of heat and mass transfer—I. Pure oscillating flow, Int. J. Heat Mass Transfer 36 (8) (1993) 2183–2192.

[28] R.M. Fand, P. Cheng, The influence of sound on heat transfer from a cylinder in cross flow, Int. J. Heat Mass Transfer 6 (1963) 571–596.

[29] M.Y. Ha, S. Yavuzkurt, A theoretical investigation of acoustic enhancement of heat and mass transfer—II. Oscillating flow with a steady velocity component, Int. J. Heat Mass Transfer 36 (8) (1993) 2193–2202.

[30] D. Karanth, G.W. Rankin, K. Sridhar, A finite difference calculation of forced convective heat transfer from an oscillating cylinder, Int. J. Heat Mass Transfer 37 (11) (1994) 1619–1630.

[31] C.H. Cheng, J.L. Hong, W. Aung, Numerical prediction of lock-on effect on convective heat transfer from a transversely oscillating circular cylinder, Int. J. Heat Mass Transfer 40 (1997) 1825–1834.

[32] C.H. Cheng, H.N. Chen, W. Aung, Experimental study of the effect of transverse oscillation on convection heat transfer from a circular cylinder, ASME J. Heat Transfer 119 (3) (1997) 474–482.

[33] E.J. Watson, Diffusion in oscillatory pipe flow., J. Fluid Mech. 133 (1983) 233–244.

[34] U.H. Kurzweg, Enhanced heat conduction in oscillating viscous flows within parallel-plate channels., J. Fluid Mech. 156 (1985) 291–300.

[35] J.G. Zhang, U.H. Kurzweg, Numerical simulation of time-dependent heat transfer in oscillatory pipe flow., AIAA J. Thermophyics and Heat Transfer 5 (1991) 401–406.

[36] M. Kaviany, Performance of a heat exchanger based on enhanced heat diffusion in fluids by oscillation: Analysis, ASME J. Heat Transfer 112 (1990) 49–55.

[37] M. Kaviany, M. Reckker, Performance of a heat exchanger based on enhanced heat diffusion in fluids by

oscillation: Analysis, ASME J. Heat Transfer 112 (1990) 56–63.
[38] Q.D. Liao, K.T. Yang, V.W. Nee, An analysis of conjugate heat transfer from a heated wall in a channel with zero-mean oscillatory flow for small oscillatory Reynolds numbers, Int. J. Heat Mass Transfer 37 (Suppl. 1) (1994) 415–423.
[39] W.L. Cooper, V.W. Nee, K.T. Yang, Experimental investigation of convective heat transfer from the heated floor of a rectangular duct to a low frequency large tidal displacement oscillatory flow, Int. J. Heat Mass Transfer 37 (4) (1994) 581–592.
[40] W.L. Cooper, K.T. Yang, V.W. Nee, Fluid mechanics of oscillatory and modulated flows and associated applications in heat and mass transfer—A Review, Journal of Energy, Heat and Mass Transfer 15 (1993) 1–19.
[41] Wetzel M, Herman C Design issues of a thermoacoustic refrigerator and its heat exchangers. In: National Heat Transfer Conference, ASME-HTD, Houston, Texas, 1996. 331. p. 137–144.
[42] A.S. Worlikar, O.M. Knio, Numerical simulation of a thermoacoustic refrigerator. Part I: Unsteady adiabatic flow around the stack, J. Comput. Phys. 127 (1996) 424–451.
[43] G. Mozurkewich, Heat transfer from a cylinder in an acoustic standing wave, J. Acoust. Soc. Am. 98 (4) (1995) 2209–2216.
[44] A. Gopinath, A.F. Mills, Convective heat transfer from a sphere due to acoustic streaming, ASME J. Heat Transfer 115 (1993) 332–341.
[45] H. Honji, Streaked flow around an oscillating cylinder, J. Fluid Mech. 107 (1981) 509–520.
[46] P. Hall, On the stability of the unsteady boundary layer on a cylinder oscillating transversely in a viscous fluid, J. Fluid Mech. 146 (1984) 347–367.
[47] W.P. Raney, J.C. Corelli, P.J. Westervelt, Acoustical streaming in the vicinity of a cylinder, J. Acoust. Soc. Am. 26 (6) (1954) 1006–1014.
[48] P.J. Westervelt, Effect of sound waves on heat transfer, J. Acoust. Soc. Am. 32 (3) (1960) 337–338.
[49] W.L. Nyborg, Acoustic streaming, in: W. Mason (Ed.), Physical Acoustics, vol. IIB, Academic Press, New York, 1965, pp. 266–331.
[50] N. Riley, Oscillatory viscous flows. Review and extension, IMA J. Appl. Math. 3 (1967) 419–434.
[51] J.T. Stuart, Double boundary layers in oscillatory viscous flows, J. Fluid Mech. 24 (1966) 673–687.
[52] N. Riley, Acoustic streaming, in: M.J. Crocker (Ed.), Encyclopedia of Acoustics, Wiley, 1997, pp. 321–327 chapter 30.
[53] T. Sarpkaya, Force on a circular cylinder in viscous oscllatory flow at low Keulegan–Carpenter numbers, J. Fluid Mech. 165 (1986) 61–71.
[54] A. Gopinath, A.F. Mills, Convective heat transfer due to acoustic streaming across the ends of a Kundt tube, ASME J. Heat Transfer 116 (1994) 47–53.
[55] N. Riley, On a sphere oscillating in a viscous fluid., Quart. J. Mech. Appl. Math. 19 (4) (1966) 461–472.